JOURNAL OF MATERIALS SCIENCE 25 (1990) 4717–4725

Crystallization in Ni–Si–B glass: the influence of dispersoid additions

M.-H. ZUERCHER, D. G. MORRIS
Institute of Structural Metallurgy, University of Neuchâtel, 2000 Neuchâtel, Switzerland

Crystallization processes in an Ni–Si–B metallic glass have been examined both for the glass alone and for the glass containing a distribution of fine crystalline particles. In the absence of dispersoids, nucleation of crystals occurs uniformly throughout the glass volume on heating following an initial slow, transient period. Nucleation occurs preferentially at the glass–dispersoid interface for the particle-containing glasses. The rate of nucleation at the dispersoid–particle interface depends on the nature of the particle and can best be correlated with the degree of misfit between the substrate and nucleating crystal for the planes and orientation relationships considered. The rate of nucleation at the dispersoid surface is shown to be completely explained on the basis of the classical heterogeneous nucleation model. Nucleation in the bulk occurs many orders of magnitude faster than predicted by classical homogeneous nucleation: the implication of this on the interpretation of nucleation is discussed.

1. Introduction

Whilst much of the interest in metallic glasses is actually fundamental in nature, for example allowing a frozen, disordered alloy to be studied, there are nevertheless many industrial applications of this class of material [1]. Interesting or attractive properties are not exclusively limited to the amorphous phase, but also apply to partially crystallized material, for example crystallized at the surface [2], or to materials containing immiscible particles distributed throughout the bulk. In this context, good control of crystallization is of prime importance, firstly in relation to obtaining optimum properties following a partial or localized crystallization or secondly because crystallization ultimately determines the stability or useful range of a glass.

A study of crystallization mechanisms is of interest because the process takes place far from equilibrium where high driving forces may lead to the selection of alternative transformation paths including, for example, the formation of metastable phases. An advantage of using metallic glasses for such a study is that the kinetics are generally very slow allowing easier control and measurement of the important parameters.

An area remaining poorly understood is that of nucleation mechanisms in such materials. Whilst the classical formulae describing homogeneous and heterogeneous nucleation are well established, the relevance of these mechanisms to glass crystallization is not clear. In many studies, for example, a clear distinction between homogeneous or heterogeneous nucleation cannot be made, neither on the basis of kinetic nor microstructural examinations.

In the present work, nucleation kinetics have been examined on ribbons of the same composition as that reported earlier [3], namely Ni–7 at % Si–17 at % B. In the present study, nucleation in the bulk, quenched glass has been examined in further detail and over a wider temperature range to allow improved precision of data and analysis. In addition, nucleation has been studied at the surface of fine, immiscible particles distributed in the bulk. Such heterogeneous nucleation on these particles is of interest because it can be used to further the understanding of nucleation occurring in the glass without deliberately added particles. Further, there is a technological interest in obtaining a glassy composite ribbon (containing immiscible particles with good adherence to the matrix) in order to obtain improved mechanical or magnetic properties, unobtainable otherwise [4].

According to the classical nucleation theory, homogeneous and heterogeneous nucleation rates can be described as

$$I_v = \frac{DN_v}{a^2}\exp\left(\frac{-\Delta G^*}{RT}\right) = \frac{D_0 N_v}{a^2}\exp\left(\frac{-\Delta G_g}{RT}\right) \times \exp\left(\frac{-\Delta G^*}{RT}\right) \quad (1)$$

and

$$I_s = \frac{DN_s}{a^2}\exp\left(\frac{-\Delta G^* f(\theta)}{RT}\right) = \frac{D_0 N_s}{a^2}\exp\left(\frac{-\Delta G_g}{RT}\right)\exp\left(\frac{-\Delta G^* f(\theta)}{RT}\right) \quad (2)$$

where I_v and I_s are the nucleation rates per unit volume and area, respectively, and D is the diffusivity or atomic mobility at the nucleus–glass interface and may be expressed using a pre-exponential term D_0 and an activation energy term ΔG_g. N_v is the number of sites

0022–2461/90 $03.00 + .12

(atoms) per volume and N_s the number per surface, a is the atomic size, R and T are the gas constant and temperature. $f(\theta)$ depends on the wetting angle θ of the crystal nucleus on the substrate and may be written [5]

$$f(\theta) = \tfrac{1}{4}(2 - 3\cos\theta + \cos^3\theta) \quad (3)$$

ΔG^* is the activation energy barrier to homogeneous nucleation and may be written

$$\Delta G^* = \frac{16\pi\gamma^3}{3\Delta G_v^2} \quad (4)$$

where γ, the crystal–glass interface energy, and ΔG_v, the volume free energy change on crystallizing, may both be expressed in terms of fundamental material parameters [6].

A practical implication of the simple relationships for homogeneous and heterogeneous nucleation (Equations 1 and 2) is that a measurement of heterogeneous nucleation kinetics together with the geometry of a nucleating crystal sitting on the substrate, that is determining the wetting angle θ, makes it possible to deduce information on the homogeneous nucleation process and its kinetics. This has been one of the objectives of the present study, namely to obtain values of ΔG^* for homogeneous nucleation based on a detailed examination of heterogeneous nucleation kinetics and geometry. At the same time it is interesting to compare the rates of heterogeneous nucleation at different dispersoid particle surfaces in an attempt to understand the factors controlling the heterogeneous nucleating efficiency of each type of particle.

2. Experimental procedure

All the samples studied in the present work were prepared by melt-spinning under well-controlled experimental conditions using the Ni–7 at % silicon–17 at % boron as base alloy. Preparation techniques have been described in detail previously [3] and are not repeated here.

The ribbons containing fine dispersoid particles in the bulk were prepared following the same melt-spinning procedure, but using a pre-mixed alloy. This alloy was prepared by melting together in a sealed quartz tube under vacuum a piece of the ternary alloy and a small quantity of the chosen particles (carbides, borides or oxides). The tube was heated to 1130 to 1150° C, about 50 to 70° C above the melting temperature, removed from the furnace and vigorously shaken during cooling to ensure that the particles were mixed uniformly throughout the alloy.

Particles suitable for inserting into the alloy must meet certain criteria: their melting temperature and thermal stability must be sufficiently high, and their solubility negligible in the alloy in order to maintain its composition. A choice of particles among carbides, nitrides and oxides was made as wide as possible in order to have nucleation sites with very different characteristics. The selected particles are shown in Table I together with some of their important characteristics. Many of the particles selected, particularly those of very high stability (enthalpy of formation exceeding 200 kJ mol^{-1}), presented very poor wetting by the melt indicating a high surface energy, and consequently were very difficult to inject in the bulk alloy. Two other particles (SiC and Mo_2C) showed a tendency to dissolve in the molten alloy and were consequently eliminated. As such, crystallization studies were eventually carried out on five different types of particles, WC, TaC, TiC, W_2C and SiO_2. Despite the difficulties of injecting this last oxide particle, it was used for study because it represents a highly possible heterogeneous nucleation site within the initial ternary alloy.

TABLE I List of particle species attempted for inclusion within the NiSiB ingots

Particle	Melting temperature, T_m (° C)	Density (g cm^{-3})	Structure	Stability (kJ mol^{-1})
WC	2780	15.8	hex.	37.7
TiN	2930	5.4	cub.	336.6
TiC	3065	4.9	cub.	183.8
AlN	> 2200	3.3	hex.	318.6
W_2C	2730	17.3	orthor.	26.4
Al_2O_3	2050	4.25	hex.	1678
SiO_2	1726	2.5	am., hex., cub.	911
SiC	2700	3.2	hex., cub.	67.0
TaC	3915	14.5	cub.	143.6
TaN	3090	14.1	hex.	252.4
Mo_2C	2690	9.2	hex.	17.6
Cr_2O_3	2266	5.21	hex.	1130
BN	3000	2.27	cub., hex.	2541

For all the ribbons containing particles, heterogeneous nucleation was studied by scanning electron microscopy on samples metallographically polished and lightly etched in order to remove the amorphous phase. This method of preparation worked particularly well for the WC particles and it was possible to examine in more detail the anisotropy of heterogeneous nucleation around the particle surface, the kinetics of nucleation over a range of temperature, as well as the wetting angle of nucleation.

3. Results

3.1. Nucleation and growth kinetics in the reference material

In the earlier publication [3], the nucleation and growth kinetics were measured at three different annealing temperatures on a ribbon quenched at an intermediate wheel speed. These results were used to determine activation energies for nucleation and growth but the analysis was subject to considerable uncertainty because of the limited experimental data. In Figs 1 and 2 the data are presented with additional results now covering the temperature range 400 to 490° C. Crystal numbers and sizes can be described by straight lines at each temperature indicating a constant and continuous nucleation and growth process. For nucleation, however, constant rates are seen only after an initial incubation period which decreases in value at higher temperatures. The continuous nucleation rates seen in Fig. 1 are not sufficient to conclude that homogeneous nucleation occurs, but the appearance of a well-defined incubation period before the nucleation rate reaches the steady-state value is a clear indication of the difficulty in establishing uniform

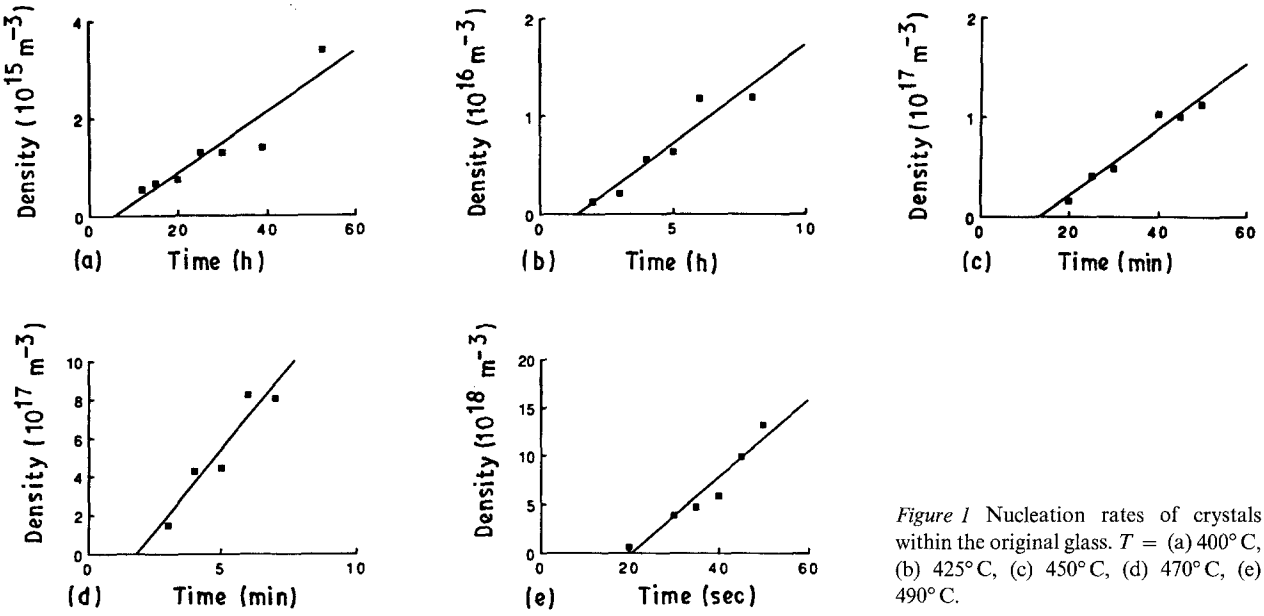

Figure 1 Nucleation rates of crystals within the original glass. T = (a) 400° C, (b) 425° C, (c) 450° C, (d) 470° C, (e) 490° C.

nucleation. The constant growth rates at each temperature seen in Fig. 2 suggest a polymorphic crystallization mechanism of a single phase. TEM studies confirm that single-phase, twinned orthorhombic crystals of Ni_3B are formed [3].

3.2. Crystal nucleation at the particle–glass interface

Fig. 3 shows examples of WC particles within a slightly crystallized glass. Several crystals at the WC–glass interface are indicated by arrows. The crystallographic orientations of the WC facets are clearly identifiable because of the hexagonal WC structure. It is also clear that nucleation occurs readily on the prismatic facets of the WC particle but very slowly on the basal plane. Crystal density and size measured on the WC particles (prismatic faces) are shown in Figs 4 and 5. The experimental uncertainty is larger in this case than on the original ribbons and rates of nucleation and growth can be reasonably defined to within a factor of two. Nucleation and growth rates are again constant at each temperature throughout all the crystallization process. Furthermore, the incubation period before nucleation has now completely disappeared and it is reasonable to conclude that nucleation begins immediately on annealing.

The study of heterogeneous nucleation on the different particles W_2C, TaC, TiC and SiO_2 was conducted only at 450° C. Fig. 6 gives an example of crystals forming on a TaC particle after annealing at 450° C. Observations on the SiO_2 particle proved to be difficult, and in fact no heterogeneously nucleated crystals were observed for any annealing treatment. The total particles (prismatic faces) are shown in Figs 4 and 5. The experimental uncertainty is larger in this case than on the original ribbons and rates of nucleation and growth can be reasonably defined to within a factor of two. Nucleation and growth rates are again constant at each temperature throughout all the crystallization process. Furthermore, the incubation period before nucleation has now completely disappeared and it is reasonable to conclude that nucleation begins immediately on annealing.

The wetting angle, θ, of a crystal at the particle–glass interface was measured from micrographs such as those of Figs 3 and 6. Such measurements were

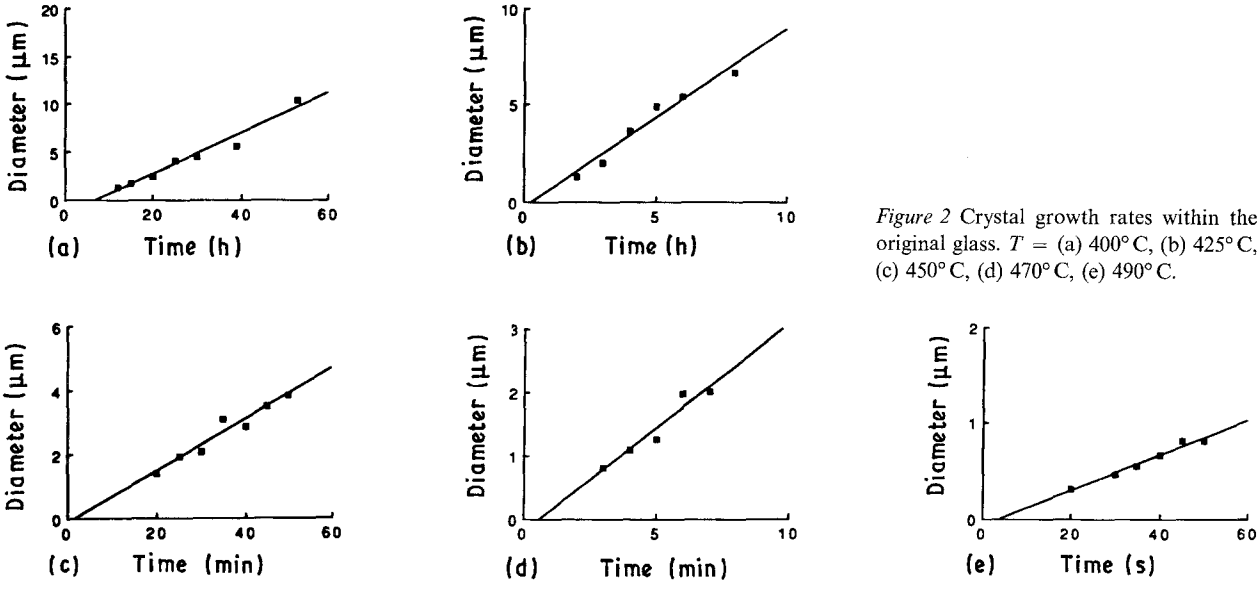

Figure 2 Crystal growth rates within the original glass. T = (a) 400° C, (b) 425° C, (c) 450° C, (d) 470° C, (e) 490° C.

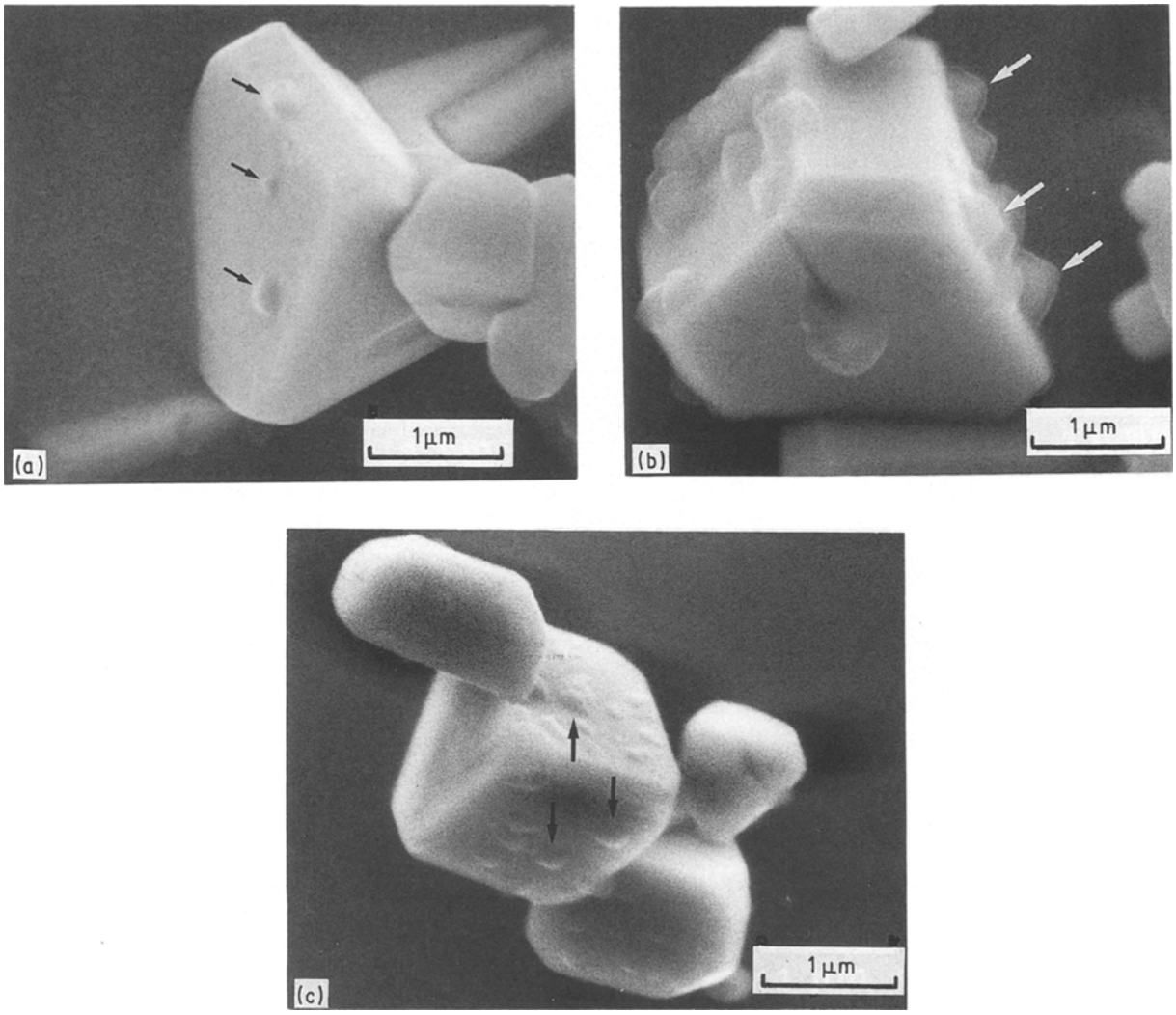

Figure 3 Crystals forming on WC particles on annealing a glass containing these particles. The polished surface has been lightly etched after polishing to remove the glassy matrix from around the particle. Note how crystal nucleation is much faster on prismatic faces than on the triangular basal plane. The wetting angle, θ, is measured on crystals when the particle face is seen end-on. Scanning electron micrographs.

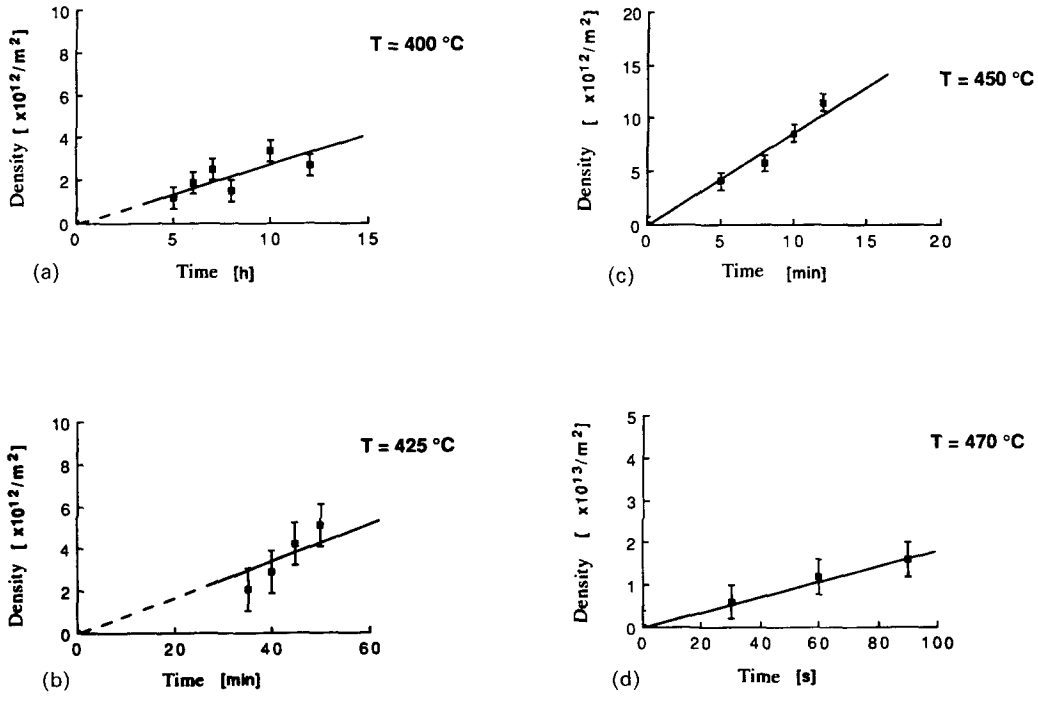

Figure 4 Crystal nucleation rate on WC particles. T = (a) 400° C, (b) 425° C, (c) 450° C, (d) 470° C.

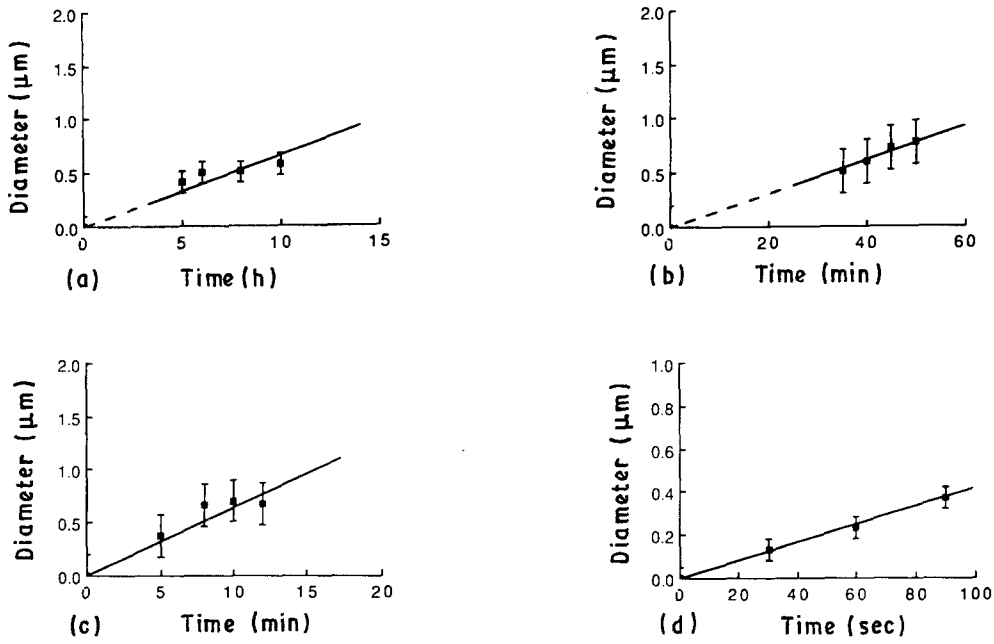

Figure 5 Crystal growth rate on WC particles. T = (a) 400° C, (b) 425° C, (c) 450° C, (d) 470° C.

made on up to 40 crystals for each particle and for those crystals oriented within the microscope such that the particle surface is parallel to the electron beam (the particle surface is seen edge-on in the micrograph). Because of difficulties in imaging very small crystals and defining profiles it was, however, only possible to measure θ for WC and TaC particles. The measured values of θ are included in Fig. 7.

4. Discussion

4.1. Analysis of nucleation and growth rates – activation energies

From the nucleation and growth kinetics shown in Figs 1 and 2 for the original glass and in Figs 4 and 5 for crystals forming on the WC particles, it is possible to determine activation energies for nucleation and growth rates, as shown, for example, in Fig. 8. Equations 1 and 2 are used to examine nucleation, and for growth

$$U = \frac{D}{a}\left[1 - \exp\left(\frac{-\Delta G_v}{RT}\right)\right] \simeq \frac{D_0}{a}\exp\left(\frac{-\Delta G_g}{RT}\right) \quad (5)$$

where U is the growth rate and D the diffusivity, which may be rewritten as

$$D_0 \exp\left(\frac{-\Delta G_g}{RT}\right)$$

For the original glass the activation energy for nucleation is 781 ± 56 kJ mol^{-1} and that for growth ΔG_g is 274 ± 10 kJ mol^{-1}. The activation energy for forming the critical nucleus, ΔG^*, is then 507 ± 57 kJ mol^{-1}. It may be seen that the Arrhenius plot of nucleation in Fig. 8 gives, in fact, a slightly curved line. The Arrhenius plot assumes that a given activated process operates with a constant value of the activation energy. Equation 4 shows that ΔG^* is, in fact, dependent on γ and ΔG_v, both of which are known to vary with temperature [6]. Inserting typical variations of γ and ΔG_v into Equation 4 shows that over the range of temperature studied, 400 to 490° C, the observed slight curvature of the Arrhenius line is well explained.

The kinetic data relating to crystals forming at the WC particles (prismatic faces) indicate activation energies for nucleation and growth of 457 and 314 kJ mol^{-1}, respectively. Making use of Equations 2 and 3, and the measured wetting angle of crystals growing on WC, 70° ± 5°, the activation energy for forming the critical nucleus (in the bulk) may be re-estimated as 564 kJ mol^{-1}.

The nucleation data of Figs 1 and 4 also show useful information on incubation times before steady state nucleation rates are achieved. In particular, the incubation times clearly apparent in Fig. 1 for nucleation in the bulk can be used to determine an activation energy for the transient stage, whilst nucleation on the WC particles begins without any clear incubation period. The variation of incubation times (bulk) with temperature depends essentially on the activation energy for a growth-like process [7, 8], and the activation energy determined, 332 kJ mol^{-1}, should be

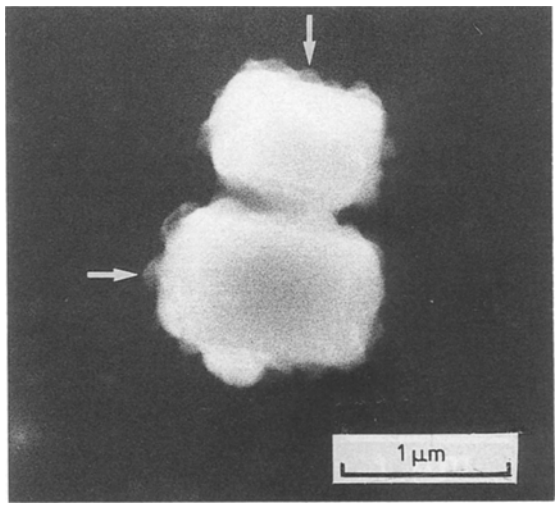

Figure 6 Crystals forming on TaC particles on annealing a glass containing the particles. The polished surface is shown without etching. Scanning electron micrograph.

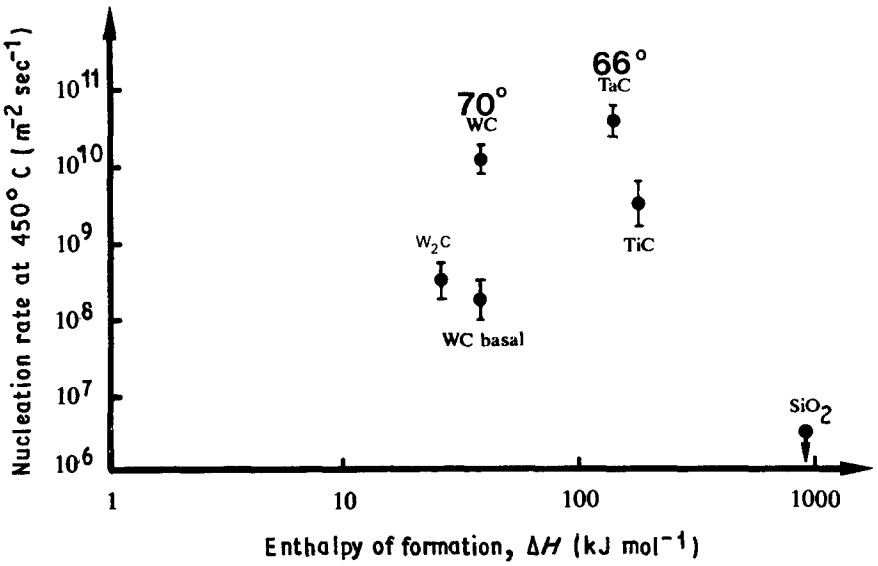

Figure 7 Crystal nucleation rates for heterogeneous nucleation at the surfaces of the various particles examined. Values of the wetting angle θ are shown where these were measured.

compared with that for growth in the bulk glass, namely 274 kJ mol^{-1}. For the moment it is not clear whether these values should be described as essentially the same, apart from experimental error, or as significantly different.

4.2. Analysis of nucleation rates in the bulk and on WC particles

More detailed analysis of nucleation and growth rates may be made by using Equations 1 to 5 and attempting a complete solution of the equations from first principles. In the following discussion this will be done firstly for crystals forming on WC substrates and then for crystals forming in the bulk glass.

Firstly, the diffusivity at a given temperature may be estimated using Equation 5. It should be noted that the crystal growth rate was the same, within experimental error, on a WC substrate and in the bulk, at a given temperature confirming that the same growth mechanisms and kinetics apply. Next, Equations 3 and 4 are used, taking reasonable values for the material parameters [5] used to estimate γ and ΔG_v-values of γ and ΔG_v of 0.25 J m^{-2} and 5.5 $\times$ 10^8 J m^{-3} are obtained. Finally, Equation 2 can be used inserting the experimentally observed heterogeneous nucleation rates, to deduce diffusion rates corresponding to the nucleation process. These "nucleation" diffusion rates are found to be very similar to the "growth" diffusion rates – the first values are 10^2 to 10^3 higher than the second. This similarity in diffusion rates is taken as good agreement, particlarly when it is seen that a variation of the experimental wetting angle θ from 70° to 60° is more than sufficient to bring the two diffusion rate estimates into perfect agreement. In summary, it follows that both the activation energy for crystal nucleation on WC and the absolute value of the heterogeneous nucleation rate are in excellent agreement with basic theory.

An equivalent analysis of the nucleation rates in the bulk glass, using Equations 1, 4 and 5 leads to very different results. The "nucleation" diffusion rates are faster than the "growth" diffusion rates by a factor of about 10^{26}. The "nucleation" diffusion rates are deduced to be about 10^6 to 10^8 m^2 sec^{-1}, which are physically unrealistic. It is clear that the simple homogeneous nucleation model, assuming a continuous process of embryo creation and activation to a stable nucleus, is insufficient to explain the results. Two possible explanations can be suggested to interpret the excessively fast nucleation kinetics. Firstly, that during an initial annealing period, for example as excess free volume anneals out, there is a stage of very fast diffusivity and it is here that a given embryo population is established. This hypothesis would imply a lower activation energy for the transient stage than for the steady state nucleation stage. A

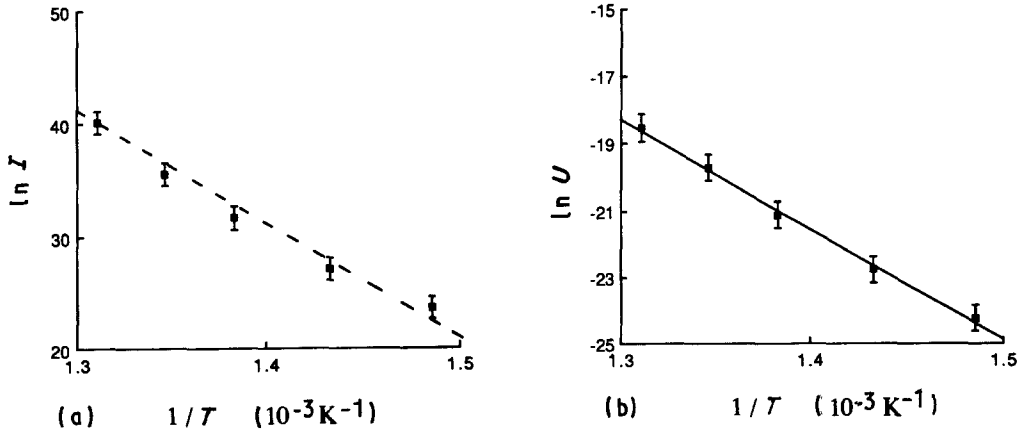

Figure 8 Arrhenius plots showing (a) nucleation and (b) growth rate data for crystal formation in the bulk glass.

second explanation is that nucleation involves a diffusion mechanism different from that of later growth, for example the co-operative movement of several atoms to form a nucleus. This hypothesis would imply a higher activation energy for the transient stage than for later growth. The experimental values, 332 kJ mol^{-1} for the transient stage and 274 kJ mol^{-1} for the growth process, suggest the second hypothesis to apply, but in fact the two activation energies are sufficiently similar to make further analysis uncertain.

4.3. Heterogeneous nucleation or homogeneous nucleation in the bulk glass?

It is interesting to examine the nucleation rates observed taking place heterogeneously, on deliberately injected particles, and to relate these to nucleation rates observed within the bulk glass.

A first point is to consider the validity of Equation 2 to describe nucleation on a substrate. This equation assumes that nucleation takes place uniformly and randomly on the substrate, and the heterogeneous nucleation rate can be related to homogeneous nucleation simply by the wetting angle, θ, which depends particularly on the degree of misfit at the crystal–substrate interface. Experimentally, within the limits of resolution of the techniques used, nucleation was seen to be random on a particle interface of a given type. Differing nucleation rates on different particle types, and between different crystallographic facets of a given particle (basal plane and prismatic plane for WC), are then explained in terms of different wetting angles. According to this interpretation the values of ΔG^* deducted using Equations 1 and 2 should be identical. The experimental values, 507 kJ mol^{-1} from bulk nucleation data and 564 kJ mol^{-1} from heterogeneous nucleation data on WC, are sufficiently close to support this idea. The two experimental tests suggest that the heterogeneous nucleation observed on the WC substrate can effectively be described using the classical nucleation model.

The question arises whether the bulk nucleation is really homogeneous, or is it possible that some other heterogeneity within the bulk glass may be responsible for the observed bulk nucleation? The similarity of the two values of ΔG^* referred to above means that any possible heterogeneity must be a weak catalyst and cause a much slower nucleation rate than WC. As an example, we can consider heterogeneous nucleation on SiO_2 particles quenched into the original glass after oxygen contamination of the alloy. The information obtained on heterogeneous nucleation on an SiO_2 substrate, shown in Fig. 7, provides a definitive answer in this case: even considering a large volume fraction of SiO_2 contaminant in the form of nanometre-sized particles, the heterogeneous nucleation rate is too low to account for the observed bulk nucleation. We can thus conclude that the observed bulk nucleation is indeed intrinsic to the alloy, and not determined by heterogeneities or impurities [10].

4.4. Heterogeneous nucleation rates on different particles

As discussed earlier, the rate of heterogeneous nucleation of crystals at the particle–glass interface should be analysed in terms of the equilibrium of interface energies and in particular in terms of the wetting angle θ and the substrate–crystal interface energy. The final point follows from the consideration that the other interfaces involved, substrate–glass and crystal–glass, are essentially incoherent and independent of substrate type. In considering such heterogeneous nucleation to take place uniformly on the substrate it is also clear that irregularities on the substrate (for example dislocations or ledges [9]) do not play a role.

The experimental data on heterogeneous nucleation rates, Fig. 7, are generally consistent with the statement above. The observed heterogeneous nucleation rate is higher for smaller values of θ, implying better wetting of the nucleating crystal on the substrate and a lower energy barrier inhibiting nucleation. However, difficulties in measuring θ mean that crystals forming on only two of the substrates were analysed in this way.

Instead, we attempt an estimate of the relative substrate–crystal interface energies based on atomic mismatch of the different crystal structures and crystallographic planes. The procedure adopted has been to superpose manually a plot of atomic positions for a chosen substrate (crystal structure and crystallographic plane) on to a plot of atomic positions for a chosen plane of the Ni_3B orthorhombic crystal. The crystal structures of the substrates (WC, W_2C, TaC, TiC and SiO_2) are known, as are the crystallographic natures of many of the substrate facets based on the observed shape and symmetry of the facets (for example basal and prismatic facets for WC, cube planes for TaC and TiC). The nucleating orientations

TABLE II Best fits found between substrates and Ni_3B crystals. Fitting is estimated as the percentage difference of atomic spacing along two orthogonal directions in the substrate–crystal interface, and as the number of atoms at the interface with a misfit of less than 15%. The rate of heterogeneous nucleation is given for comparison

Particle	Difference in atomic spacing along two directions (%)	Number of atoms with misfit less than 15%	Nucleation rate at 450° C ($m^{-2} sec^{-1}$)
TaC	1 and 5	> 100	6×10^{10}
WC (prismatic plane)	8 and 14	30–40	1×10^{10}
WC (basal plane)	10 and 14	10–12	2×10^{8}
W_2C	7 and 15	15	6×10^{8}
SiO_2	No coherence	–	$< 5 \times 10^{6}$

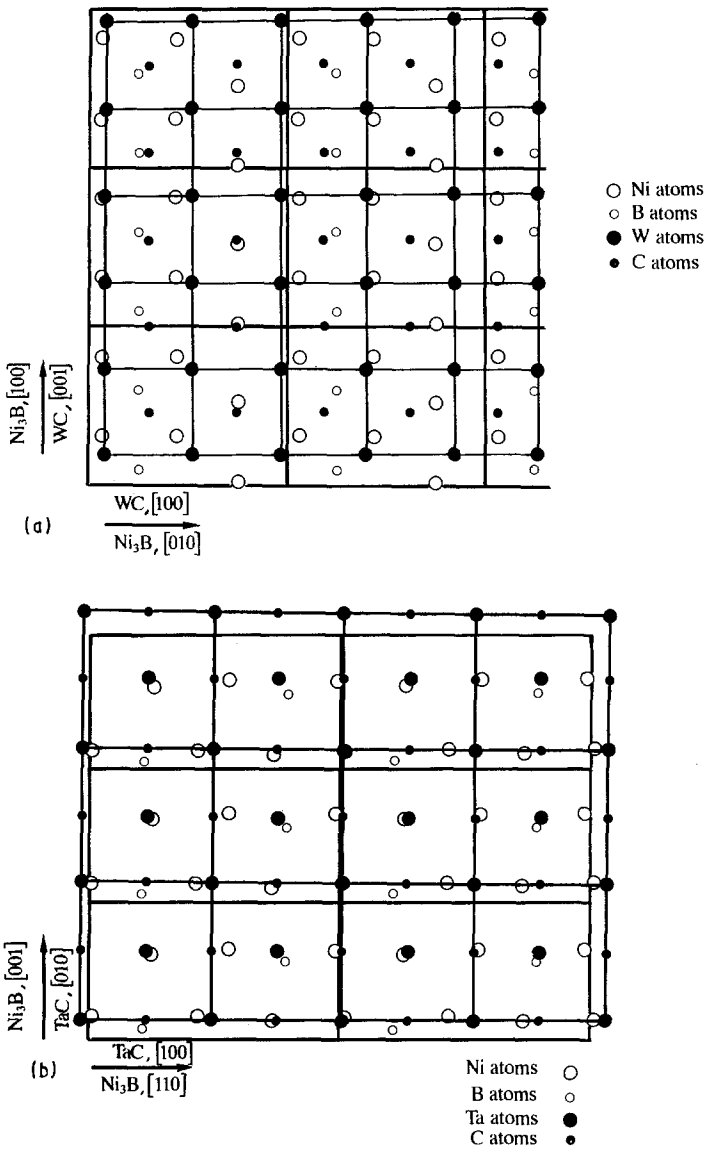

Figure 9 Examples of best atom fitting discovered for an Ni_3B orthorhombic crystal sitting on (a) WC, prismatic plane substrate, and (b) TaC, cube plane substrate. In (a) the Ni_3B crystal has the (0 0 1) orientation and in (b) the (1 $\bar{1}$ 0) orientation.

of the Ni_3B crystals are not known, and the procedure adopted has been to search for the best fit orientation of Ni_3B on a given substrate facet by considering all low-index orientations ($h\,k\,l$) on Ni_3B up to the level $h + k + l = 5$. The task was made easier by the use of a computer programme to plot atomic positions for a given crystallographic structure and plane. Examples of fitting for a WC, prismatic plane substrate and a TaC, cube plane substrate are shown in Fig. 9. Finally, Table II summarizes the data on degree of misfit obtained by such analysis, shown as the misfit along two orthogonal directions at the interface and as the number of atoms that can be deposited on the substrate plane with a misfit of less than 15% (arbitrary chosen value). It is seen that the observed heterogeneous nucleation rate varies in a consistent manner with the degree of misfit, implying a causal relationship between the data.

5. Conclusions

A detailed study of crystallization rates associated with a uniform NiSiB glass and also with the same glass containing a dispersion of various stable particles makes possible a better understanding of crystal formation within the bulk as well as, heterogeneously, on the surfaces of the included particles.

The similarity of activation energies for nucleation (ΔG^*) in the bulk and on a substrate, after taking account of the $f(\theta)$ term, tends to suggest that nucleation in the bulk is really homogeneous in character, and unaffected by any pre-existing particle or impurity. Whilst the absolute value of heterogeneous nucleation rate is completely explained, quantitatively, by classical theory, the rate of nucleation in the bulk glass is many orders of magnitude higher than theory suggests. The explanation for this excessively fast nucleation is not clear, but may involve a different diffusional mechanism, such as coupled atom movement, during the early stage of creation of a nucleus.

The rate of nucleation on a heterogeneity such as an included particle depends on the substrate–crystal interface energy or wetting, which can reasonably well be related to the degree of atom misfit at the interface between the two crystal structures.

Acknowledgements

We thank Dr P. Stadelmann, IIM, Swiss Federal Technical School, Lausanne, for the use of his computer program for determining atom positions in a given crystal structure, and Dr M. Morris for assistance with scanning electron microscopy. This work was funded by the Swiss National Science Foundation.

References

1. F. E. LUBORSKY, (Ed.) "Amorphous Metallic Alloys" (Butterworths, London, 1983).
2. H. WARLIMONT, in "Proceedings of the 6th International Conference on Rapidly Quenched Metals", Vol. 3, edited by R. W. Cochrane and J. O. Ström-Olsen (Elsevier Applied Science, London, New York, 1988) pp. 1–11.
3. M.-H. ZUERCHER and D. G. MORRIS, *J. Mater. Sci.* **23** (1988) 515.
4. H. KIMURA, T. MASUMOTO and D. G. AST, *Acta Metall.* **35** (1987) 1757.
5. D. A. PORTER and K. E. EASTERLING, "Phase Transformations in Metals and Alloys" (Van Nostrand Reinhold, Wokingham, 1983).
6. C. V. THOMPSON and F. SPAEPEN, *Acta Metall.* **27** (1979) 1855.
7. J. W. CHRISTIAN, "The Theory of Transformations in Metals and Alloys", 2nd Edn, International Series on Materials Science and Technology (Pergamon Press, Oxford, 1975) pp. 442–8.
8. C. V. THOMPSON, A. L. GREER and F. SPAEPEN, *Acta Metall.* **31** (1983) 1883.
9. M.-H. ZUERCHER and D. G. MORRIS, *J. Less-Common Metals* **145** (1988) 167.
10. M.-H. ZUERCHER, Doctoral Thesis, Institute of Structural Metallurgy, University of Neuchâtel, Switzerland (1989) (in French).

Received 13 June
and accepted 22 November 1989